Implications for Ocean Mixing of Internal Wave Scattering off Irregular Topography

DENIS GILBERT AND CHRISTOPHER GARRETT

Department of Oceanography, Dalhousie University, Halifax, NS, Canada

(Manuscript received 11 April 1989, in final form 8 June 1989)

ABSTRACT

Earlier work has suggested that internal wave reflection off sloping bottoms may cause significant diapycnal mixing in the deep ocean, and may also represent an important sink of internal wave energy. Most theories have been limited, however, by the representation of the bottom as an infinite plane slope. In this paper, the scattering of internal waves off irregular topography is studied for a few idealized bottom shapes. We pay special attention to the critical case, which occurs when the bottom slope dh/dx locally matches the wave ray slope s. Analytical solutions for bottom shapes such that $dh/dx = s$ at a single point are discussed for both locally convex and concave topography, and are compared with the results of specular reflection theory. They lead to the important conclusion that one is more likely to observe energy enhancement at the critical frequency above locally convex rather than concave topography. This suggests that energy dissipation rates associated with the breaking of internal waves may also be higher above locally convex topography. We also note that, for locally convex topography, rapid variations of the reflected wavefield with height above the bottom can be explained by purely geometric effects, and need not be a consequence of nonlinear interactions.

1. Introduction

When internal waves reflect off a sloping bottom, their frequency is conserved and hence the magnitude of the angle which the wave rays make with the horizontal is also conserved. Close to the critical frequency ω_c at which the wave ray slope is equal to the bottom slope, simple kinematics (Phillips 1977) show that, upon reflection, the wavenumber, energy density, and shear associated with the incident waves are greatly amplified, so that shear instability and energy dissipation are more likely. Eriksen (1982) has presented observational evidence for energy and shear enhancement near the critical frequency at a few mooring sites. He also observed Richardson numbers close to ¼ (and hence a presumption of shear instability) over vertical scales of 40–50 m in the first 100 m above the bottom at mooring 636 of the Western Boundary Sill Experiment (4°2′N, 39°40′W), which is suggestive of intense mixing near the bottom at this location. These observations led Eriksen (1985) to explore some of the possible implications for ocean mixing of the shear instability of internal waves reflected off a sloping sea floor.

Using the observational requirement that the internal wave spectrum a few hundred meters above a sloping bottom has seemingly readjusted to the canonical GM79 form (Munk 1981), Eriksen computed a quantity which he called the "redistributed energy flux" normal to the bottom. He defined it as the integral over all azimuths, frequencies, and wavenumbers of the modulus of the difference between the reflected energy flux and what this flux would be for a reflected spectrum of canonical form. The values he obtained for the redistributed energy flux were so large (20–30 mW m^{-2}) that only a small fraction of it would be sufficient to maintain a coefficient of vertical eddy diffusivity K_v of 10^{-4} m^2 s^{-1} in the ocean. However, a major shortcoming with Eriksen's calculation of the "redistributed energy flux" was that he offered no explicit criteria to say how much of it should be lost to dissipation, the remainder being presumably redistributed in the four-dimensional internal wave spectrum by nonlinear processes. In any event, it seems very unlikely that the energy flux lost from the internal wave spectrum could be of the same order of magnitude as the "redistributed energy flux," since this would drain the internal wavefield of its total energy of about 4×10^3 J m^{-2} (Munk 1981) in just a few days, leading to far less universality of the internal wave spectrum in time and space than seems to be typical (e.g., Olbers 1983).

Garrett and Gilbert (1988, hereafter GG), have proposed a more specific model based on mechanistic ideas to estimate the energy flux that might be lost to dissipation. They first calculated the vertical modenumber j_p such that, for a typical incident internal wave spectrum, the reflected waves have a Richardson number of order 1 if their shear spectrum is integrated from $j = 1$ to $j = j_p$. They then argued that waves reflected with $j > j_p$ are likely to undergo shear instability, and

Corresponding author address: Mr. Denis Gilbert, Dept. of Oceanography, Dalhousie University, Halifax, NS, Canada B3H 4J1.

hence break and cause mixing at a rate proportional to their bottom-normal energy flux. Their results indicate that the dissipated energy flux F_d may be of the order of 1 mW m^{-2} (Fig. 1). These estimates of F_d, while much less than Eriksen's "redistributed energy flux," still appear to be significant for deep-ocean mixing rates and may represent an important sink in the overall energy balance of the oceanic internal wavefield (Olbers 1983). It is interesting to note that for the model incident spectrum discussed by Munk (1981), the formulae obtained by GG for the cutoff mode-number j_p and the dissipated energy flux F_d depend only on the two parameters $\tan\alpha$ and f/N, where $\tan\alpha$ is the bottom slope and f/N is the ratio of the inertial to the buoyancy frequency. With regard to this, Fig. 1 shows that (i) for a given value of f/N, F_d generally increases with bottom slope $\tan\alpha$, reaching a broad maximum when $\tan\alpha \approx 3f/N$, and (ii) for a given value of $\tan\alpha$, F_d increases as f/N gets smaller, suggesting that boundary mixing via internal wave breaking should be more intense at low latitudes than at midlatitudes. This may explain why the clearest evidence of energy and shear enhancement near ω_c presented by Eriksen (1982) came from a low-latitude site.

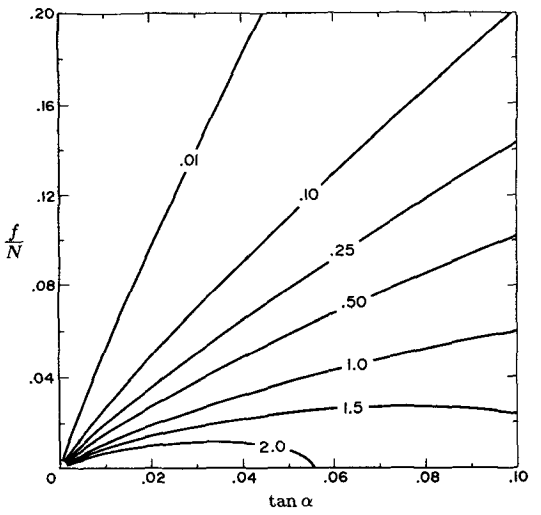

FIG. 1. Dissipated energy flux F_d, in mW m^{-2}, as a function of bottom slope $\tan\alpha$ and frequency ratio f/N (from Garrett and Gilbert 1988).

Now GG have pointed out some of the weaknesses of their model for estimating F_d. In the present paper we will be concerned with just one of these, namely their neglect of finite topographic effects. Strictly speaking, the reflection laws developed by Eriksen (1982),[1] and used by GG, are only valid for infinite sloping planes. It is therefore not obvious that they can be used to provide a good description of the interaction of internal waves with a bottom of nonuniform slope, and if so, under what conditions.

In our attempt to tackle at least some aspects of this problem, we will be particularly interested in determining how the critical reflection process is affected. For waves of a given frequency incident on a bottom of varying slope, the wave ray slope will match the local bottom slope only at a few isolated points, so we ask whether large enhancements of vertical shear and energy density near the critical frequency can still be expected in the neighborhood of these points.

In section 2, we review previous work on the scattering of internal waves off sinusoidal topography, and point out some of its limitations with regard to the critical case. In section 3, we present Baines' (1971b, 1974) exact solutions for the scattering of internal waves off locally convex and concave topography respectively, and interpret them in terms of specular reflection theory. In section 4, we extend the theory of Hurley (1970) in order to evaluate the total energy flux backscattered from a sharp convex corner. The possible significance of our result for a rounded convex corner is briefly discussed. In section 5, we present a simple model for the spatial pattern of the reflected wavefield above locally convex topography, using specular reflection theory. In section 6 we discuss the results of previous sections and summarize our main conclusions.

2. Sinusoidal topography

Baines (1971a, 1971b) has done much of the pioneering work on the scattering of internal waves by irregular topography. He pointed out the importance of using the proper form of the radiation condition, which requires the scattered waves to propagate energy away from the boundary, and showed that the correct formulation of the problem of a single wave incident on smoothly-varying topography can be written in terms of a Fredholm integral equation of the second kind. For the "flat-bump" case where the bottom slope dh/dx is everywhere less than the characteristic slope s, Baines (1971a) arrived at the surprising conclusion that the back-reflected wave (i.e., that reflected back along the incident characteristic) usually does not vanish, so that the simple application of ray theory (e.g., Longuet-Higgins, 1969) is incorrect.

A logical first step in the study of internal wave scattering by irregular topography is to investigate the problem of a single wave component incident on sinusoidal topography of infinitesimal amplitude. The solution of this problem could then be used to determine the scattered wavefield over arbitrarily complicated topography, subject to linearization of the boundary condition.

[1] Sandstrom (1966) derived an earlier version of these laws, but did not publish it.

To simplify matters, Baines (1971a) assumed that both the wave motion and the bottom topography are independent of the alongslope y-coordinate. This 2-D assumption, together with the incompressibility condition $\nabla \cdot \mathbf{u} = 0$, enabled him to describe the wave motion in terms of a streamfunction and thus facilitated analytical treatment of the problem. He let a monochromatic wave of frequency ω, characteristic slope s, and wavenumber (sK_1, K_1) in (x, z) space be incident on a sinusoidal bottom

$$h(x) = d \cos lx \tag{2.1}$$

where d is the amplitude of the sinusoidal perturbation, and l is the topographic wavenumber. Making the "flat-bump" assumption

$$\left|\frac{dh}{dx}\right|_{\max} = ld < s \quad \text{for} \quad -\infty < x < \infty \tag{2.2}$$

and assuming that $K_1 d \ll 1$ and $ld \ll 1$, Baines found that, in addition to the specularly reflected wave whose wavenumber is $(sK_1, -K_1)$, two scattered waves were generated with wavenumbers

$$\mathbf{K}' = (sK_1 \pm l, -|K_1 \pm l/s|). \tag{2.3}$$

The sum (+) wave is always forward-scattered, whereas the difference (−) wave can be either forward-scattered when $l < sK_1$ or backscattered when $l > sK_1$. Denoting by F_i the energy flux associated with the incident wave, and by $F_\pm$ the energy flux associated with the sum and difference waves, Baines showed that

$$\frac{F_\pm}{F_i} = \left|K_1 \pm \frac{l}{s}\right| K_1 d^2 \tag{2.4}$$

to first order accuracy in $K_1 d$ and ld.

In an interesting paper, Rubenstein (1988) expanded the work of Baines (1971a) by applying (2.4) to a more general bathymetric profile, using the empirical power spectrum of topographic variations introduced by Bell (1975b). The downward propagating part of the model internal wave spectrum of Munk (1981) was assumed to be incident on this rough bottom. Rubenstein found that the principal interactions involve the scattering of low-frequency, low-wavenumber incident waves into higher wavenumbers. Because of its higher wavenumbers, the scattered wavefield has elevated shear levels compared to the incident wavefield. He found that the inverse Richardson number (Ri^{-1}), summed from mode $j = 1$ to $j = 260$, is increased by a factor of about 3.6 with respect to the incident wavefield. This is important, as it shows we can expect enhanced internal wave breaking above a bumpy bottom even when the mean slope on a larger scale is effectively zero. The mechanism leading to shear enhancement here is thus somewhat different from that envisaged by Eriksen (1985) and GG, who assumed the bottom was bumpless but had a nonzero mean slope.

The conclusions of Rubenstein (1988) are probably qualitatively true. However, they are quantitatively uncertain as there are problems associated with the use of (2.4), the cornerstone of his paper. Perhaps the most serious of these is that (2.4) was obtained under the assumption that the bottom slope is everywhere less than the characteristic slope (2.2). Shadowing effects are thus strictly forbidden, and the critical case where $dh/dx = s$ locally, which is so important from a shear point of view (Eriksen 1982; GG), cannot be dealt with explicitly.

Now for "abyssal hills" topography, the rms bottom slope depends on the scale of resolution, but equals 0.07 for topographic wavenumbers less than 0.75 cycle km^{-1} according to Bell (1975a). We might stipulate, as Rubenstein did, that the flat-bump assumption ($s > dh/dx$) is then satisfied in a probabilistic sense (95% probable) for $s > 0.14$. For the "typical" midlatitude value of $N/f = 10$ (e.g., Bell 1975a), this corresponds to $\omega > 1.7f$ in the frequency domain, which leaves a wide range of near-inertial frequencies ($f < \omega < 1.7f$) for which the flat-bump assumption would be violated. The range of offending frequencies is of course very sensitive to the value of N/f; it would be reduced to ($f < \omega < 1.2f$) for $N/f \approx 5$ for instance, a fairly common situation at midlatitudes in the 4–5 km depth range.

Another problem with (2.4) is that it is only accurate to first-order in $K_1 d$ and ld. Mied and Dugan (1976) numerically performed a higher-order perturbation expansion involving a finite set of $2n_{\max} + 1$ discrete, scattered horizontal wavenumbers

$$K_x' = sK_1 \pm nl, \quad n = 0, 1, 2, 3, \cdots, n_{\max}. \tag{2.5}$$

Their higher-order solution for the scattered wavefield agrees remarkably well with the first-order solution of Baines (1971a) for $ld \leqslant s/6$, i.e., the contributions from $n \geqslant 2$ are then unimportant. However, when the bottom slope ld becomes steeper than about $s/2$, they find that the series solution (2.5) fails to converge. This is unfortunate, in that it does not take us nearly as close to the critical case as is desirable; in the model of GG, for slopes of infinite extent, it was typically found that 80% of the total shear comes from waves with ray slopes within ±20% of the critical wave ray slope.

Mied and Dugan (1976) also pointed out that (2.4) only conserves the energy flux of the incident wave to $O(K_1^2 d^2/s^2)$, so that for a given bathymetry profile for which $K_1 d$ is held fixed, Baines' solution will do much worse at conserving the energy flux of the incident wave at low frequencies than at high frequencies. This, as well as the occasional violations of the flat-bump assumption, limits the ability of (2.4) to describe

the interaction of near-inertial waves with the ocean bottom, which is what Rubenstein (1988) was primarily concerned with.

3. Local topographic effects

Given our inability to deal properly with the critical case using a Fourier representation of the topography, we can at least try to determine some properties of the scattered wavefield for particular topographic shapes.

Baines (1971b) developed a two-dimensional theory for the scattering of internal waves off smoothly varying topography, in which the critical case can be dealt with explicitly, provided $dh/dx = s$ at a single location in the bathymetry profile. Using the same radiation condition as in Baines (1971a) he was able to reduce the problem of determining the scattered wavefield to a pair of coupled integral equations with two unknown functions. He cast the problem in terms of the characteristic coordinates

$$\xi = z + sx, \quad \eta = z - sx \tag{3.1}$$

where z is the vertical (upwards) coordinate, x is the cross-isobath (onshore) coordinate, and s is the characteristic (or wave ray) slope. The origin of both the characteristic and Cartesian coordinate systems is chosen to coincide with the single location in the bathymetry profile where $dh/dx = s$. Now for smoothly varying topography, the bottom can be regarded as either locally convex ($d^2h/dx^2 < 0$) or concave ($d^2h/dx^2 > 0$). It should therefore be useful to examine the properties of the scattered wavefield for both of these cases.

a. *Locally convex topography*

For locally convex topography with radius of curvature R at the origin, Baines (1971b) showed that, for $|\xi/R| \ll 1$, the equation for the bottom can be approximated by

$$\eta = -c_1\xi^2, \quad c_1 = \frac{(1 + s^2)^{3/2}}{8s^2R} \tag{3.2}$$

in terms of the characteristic coordinates (Fig. 2). This equation is symmetric in ξ, an asymmetric term proportional to ξ^3/R^2 having been neglected. Baines let a plane wave with stream function $\psi_i = \epsilon \exp\{i(K_1\xi - \omega t)\}$ of infinitesimal amplitude ϵ, total wavenumber $K_1(1 + s^2)^{1/2}$, and frequency ω be incident on idealized topography specified exactly by (3.2). He obtained an analytical solution for the scattered wavefield, and expressed it as a superposition of a back-reflected (or backscattered) wave ψ_R, a wave transmitted to the right ψ_{Tr}, and a wave transmitted to the left ψ_{Tl} (see Fig. 2). His solution may be conveniently summarized as follows:

$$\psi_R(\xi, t) = 0, \quad -\infty < \xi < \infty \tag{3.3}$$

$$\psi_{Tr}(\eta, t) = \psi_{Tl}(\eta, t) = -\epsilon \exp\{-K_1(\eta/c_1)^{1/2}\} \exp(-i\omega t), \quad 0 < \eta < \infty \tag{3.4}$$

$$\psi_{Tr}(\eta, t) = -\epsilon \exp\{i[K_1(|\eta|/c_1)^{1/2} - \omega t]\}, \quad \xi > 0, -\infty < \eta < 0 \tag{3.5}$$

$$\psi_{Tl}(\eta, t) = -\epsilon \exp\{-i[K_1(|\eta|/c_1)^{1/2} + \omega t]\}, \quad \xi < 0, -\infty < \eta < 0. \tag{3.6}$$

It is worth analyzing this solution in some detail. The vanishing of the backscattered wave (3.3) is a property of the particular bottom shape specified by (3.2): symmetric in ξ and parabolic in the characteristic coordinates, with slope at infinity asymptotic to that of the ξ-characteristics. The backscattered wave does not necessarily vanish for other bottom shapes.

For the region above the grazing characteristic ($\eta > 0$), where purely specular reflection would produce no motion, (3.4) describes an evanescent field of oscillatory motions with velocity amplitude

$$\left|\frac{\partial\psi_T}{\partial\eta}\right| = \frac{\epsilon K_1}{2(c_1\eta)^{1/2}} \exp\{-K_1(\eta/c_1)^{1/2}\}, \quad 0 < \eta < \infty \tag{3.7}$$

where ϵK_1 is the velocity amplitude of the incident wave. The time-averaged kinetic energy density is thus given by

$$\frac{1}{4}\left|\frac{\partial\psi_T}{\partial\eta}\right|^2 = \frac{\epsilon^2 K_1^2}{16(c_1\eta)} \exp\{-2K_1(\eta/c_1)^{1/2}\}, \quad 0 < \eta < \infty. \tag{3.8}$$

The e-folding scale associated with the exponential factor in (3.8) is given by $\eta = c_1/4K_1^2 = (1 + s^2)^{3/2}/(32s^2K_1^2R) \approx (32s^2K_1^2R)^{-1}$. It is therefore very sensitive to our choice of s, K_1 and R. For example, it equals 1250 m for $K_1 = 10^{-3}$ m^{-1}, $s = 0.05$, $R = 10^4$ m, but merely equals 12.5 m for $K_1 = 10^{-2}$ m^{-1} with s and R unchanged, indicating a much faster rate of decay of the scattered wavefield for large incident wavenumbers (small incident wavelengths). Note that the distance from the $\eta = 0$ characteristic is given by $|\eta|/(1 + s^2)^{1/2}$, which approximately equals $|\eta|$ for small wave ray slopes, and that the kinetic energy density in (3.8) decays as η^{-1} for $0 < \eta \ll c_1/4K_1^2$.

In the region below the grazing characteristic ($\eta < 0$), i.e., for η-characteristics which intersect the bottom, (3.5) and (3.6) describe a field of propagating internal waves with velocity amplitude

$$\left|\frac{\partial\psi_T}{\partial\eta}\right| = \frac{\epsilon K_1}{2(c_1|\eta|)^{1/2}}, \quad -\infty < \eta < 0 \tag{3.9}$$

and time-averaged kinetic energy density

$$\frac{1}{4}\left|\frac{\partial\psi_T}{\partial\eta}\right|^2 = \frac{\epsilon^2 K_1{}^2}{16c_1|\eta|} = \frac{\epsilon^2 K_1{}^2 s^2 R}{2(1+s^2)^{3/2}|\eta|},$$

$$-\infty < \eta < 0. \quad (3.10)$$

As Baines (1971b) pointed out, perhaps the most significant feature of the field of motion (3.3)–(3.6) is that the kinetic energy density near $\eta = 0$ is proportional to $\epsilon^2 K_1{}^2 R/|\eta|$, as can be seen from (3.8) and (3.10). There is a singularity at $\eta = 0$, and the strength of this singularity increases with the local radius of curvature R ($R = \infty$ for a bottom of uniform slope). Now with $\psi_R = 0$, the condition that the total streamfunction ψ must vanish on the boundary reduces to

$$\psi_i + \psi_{Tl} = 0 \quad \text{on} \quad \xi = -(|\eta|/c_1)^{1/2} \quad (3.11)$$

$$\psi_i + \psi_{Tr} = 0 \quad \text{on} \quad \xi = (|\eta|/c_1)^{1/2}. \quad (3.12)$$

A similar boundary condition involving only incident and reflected wave components can be used to derive Phillips' (1977) law of reflection. Hence we expect the latter to be valid for $\eta < 0$, i.e., for the region of the fluid where η-characteristics intersect the bottom. To verify this, we first need to find a relationship between the bottom slope dh/dx and the characteristic coordinate ξ for the idealized topography shown on Fig. 2. Substituting $\xi = h(x) + sx$ and $\eta = h(x) - sx$ into (3.2), and differentiating with respect to x, we obtain

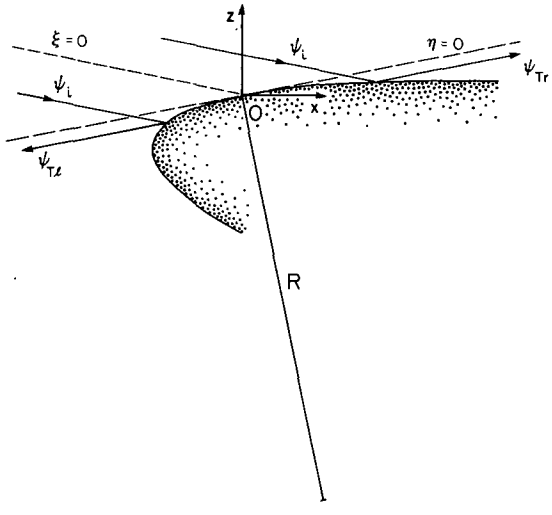

FIG. 2. A plane wave with streamfunction ψ_i is incident on topography specified by (3.2) and gives rise to a wave transmitted to the left, ψ_{Tl}, and a wave transmitted to the right, ψ_{Tr}. The backreflected wave ψ_R vanishes for this particular bottom shape. The arrows point in the direction of energy propagation, and the wave ray slope is $s = 0.2$. The origin coincides with the single location in the bathymetry profile where the bottom slope matches the wave ray slope, and R denotes the radius of curvature of the topography there. The characteristic coordinates are $\xi = z + sx$, $\eta = z - sx$.

$$\frac{dh}{dx} = \frac{s(1-2c_1\xi)}{(1+2c_1\xi)}. \quad (3.13)$$

The bottom is thus vertical at $\xi = -1/(2c_1)$, and horizontal at $\xi = 1/(2c_1)$. We also verify that $dh/dx = s$ at $\xi = 0$, and $dh/dx \to -s$ as $\xi \to \pm\infty$, as stated earlier in the text. Our next step consists of defining the phase function

$$\Phi(\eta, t) = K_1\left(\frac{|\eta|}{c_1}\right)^{1/2} - \omega t \quad (3.14)$$

for the wavefield $\psi_{Tr}(\eta, t)$ given in (3.5). Subject to the WKB approximation (Gill 1982, p. 300), a local wavenumber $K'(\eta)$ may then be defined by

$$K'(\eta) = \frac{\partial}{\partial\eta}\Phi(\eta, t) = \frac{K_1\,\mathrm{sgn}(\eta)}{2c_1{}^{1/2}|\eta|^{1/2}} \quad (3.15)$$

yielding the wavenumber amplification

$$\frac{K'}{K_1} = \frac{-1}{2c_1{}^{1/2}|\eta|^{1/2}}.$$

A similar amplification in velocity amplitude was implicit in (3.9). Now by virtue of (3.12), we can replace $|\eta|^{1/2}$ by $c_1{}^{1/2}\xi$, so that

$$\frac{K'}{K_1} = \frac{-1}{2c_1\xi}. \quad (3.16)$$

Rearranging terms in (3.13), we get

$$\xi = \frac{-(dh/dx - s)}{2c_1(dh/dx + s)} \quad (3.17)$$

and substituting this back into (3.16), we obtain

$$\frac{K'}{K_1} = \frac{(dh/dx + s)}{(dh/dx - s)}. \quad (3.18)$$

It is relatively easy to show that (3.18) is equivalent to Phillips' (1977, p. 227) formula for the wavenumber amplification. Letting $dh/dx = \tan\beta$, and $s = \tan\mu$, we get

$$\frac{K'(\eta)}{K_1(\xi)} = \frac{\sin(\beta+\mu)}{\sin(\beta-\mu)}. \quad (3.19)$$

By virtue of (3.1), the vertical wavenumber amplification is also given by (3.19), whereas the horizontal wavenumber amplification is given by the negative of that. Equation (3.19) is thus consistent with the specular reflection theory of Phillips, as could be expected from the simple form of the boundary condition (3.12). This is an important result. It suggests that when the backscattered wave either vanishes or is small enough to be neglected compared to the incident and reflected waves, then internal wave reflection off a bottom of nonuniform slope does not differ significantly from reflection off a uniform slope, the rules for which are well

known. The implications of this for ocean mixing are that for a given frequency, large enhancements of vertical shear and energy density can still be expected above locally convex topography in the neighborhood of points where $dh/dx = s$.

b. *Locally concave topography*

Using the same formalism as in Baines (1971b), Baines (1974, appendix 1) also examined the problem of internal wave scattering off locally concave topography. For $|\xi/R| \ll 1$, the equation for the bottom can be approximated by (see Fig. 3)

$$\eta = c_1\xi^2, \quad \text{where} \quad c_1 = \frac{(1+s^2)^{3/2}}{8s^2R}. \tag{3.20}$$

Substituting $\xi = h(x) + sx$ and $\eta = h(x) - sx$ into (3.20), and differentiating with respect to x, we can obtain a formula for the bottom slope dh/dx as a function of the characteristic coordinate ξ (cf. (3.13))

$$\frac{dh}{dx} = \frac{s(1+2c_1\xi)}{(1-2c_1\xi)}. \tag{3.21}$$

The topographic shape described by (3.20) is thus horizontal at $\xi = -1/(2c_1)$, and vertical at $\xi = 1/(2c_1)$. We still have $dh/dx = s$ at $\xi = 0$, and $dh/dx \to -s$ at $\xi \to \pm\infty$, as for Fig. 2. For an incident plane wave with streamfunction

$$\psi_i(\xi, t) = \epsilon \exp\{i(K_1\xi - \omega t)\}, \quad -\infty < \xi < \infty, \tag{3.22}$$

Baines' solution for the scattered wavefield may be expressed as the superposition of a back-reflected wave ψ_R and an η-dependent field of motion ψ_T, where

$$\psi_R(\xi, t) = \epsilon \exp\{-i(K_1\xi + \omega t)\}, \quad -\infty < \xi < \infty \tag{3.23}$$

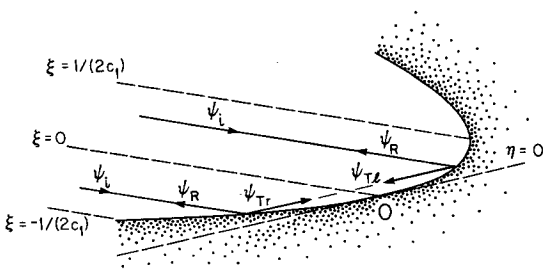

FIG. 3. As in Fig. 2, but for topography specified by (3.20). The back-reflected wave ψ_R has the same magnitude as the incident wave ψ_i, and we have a pure standing wave pattern. The bottom is vertical at $\xi = 1/(2c_1)$, and horizontal at $\xi = -1/(2c_1)$.

and

$$\psi_T(\eta, t) = -2\epsilon \cos\left\{K_1\left(\frac{\eta}{c_1}\right)^{1/2}\right\} \exp(-i\omega t), \quad 0 < \eta < \infty. \tag{3.24}$$

Perhaps the most striking feature of this solution is that the back-reflected wave ψ_R has exactly the same amplitude as the incident wave ψ_i, and since it travels in the opposite direction, a standing wave pattern results:

$$\psi_i(\xi, t) + \psi_R(\xi, t) = 2\epsilon \cos K_1\xi \exp(-i\omega t). \tag{3.25}$$

The total streamfunction $\psi = \psi_i + \psi_R + \psi_T$ is thus equal to zero for $\xi = \pm(\eta/c_1)^{1/2}$, as required by the no-normal flow boundary condition. Note that (3.24) also represents a standing wave pattern, with velocity amplitude

$$\left|\frac{\partial\psi_T}{\partial\eta}\right| = \frac{\epsilon K_1}{(c_1\eta)^{1/2}} \sin\left\{K_1\left(\frac{\eta}{c_1}\right)^{1/2}\right\} = \frac{\epsilon K_1}{(c_1\eta)^{1/2}}\left\{K_1\left(\frac{\eta}{c_1}\right)^{1/2} - \frac{K_1^3}{3!}\left(\frac{\eta}{c_1}\right)^{3/2} + \cdots\right\} \tag{3.26}$$

which, for $K_1(\eta/c_1)^{1/2} \ll 1$, reduces to (after correcting equation (A13) of Baines (1974) for a missing factor K_1^2)

$$\left|\frac{\partial\psi_T}{\partial\eta}\right| \approx \frac{\epsilon K_1^2}{c_1} = \epsilon K_1 \frac{8s^2(K_1R)}{(1+s^2)^{3/2}} \tag{3.27}$$

where ϵK_1 is the velocity amplitude of the incident wave. Interestingly enough, this velocity field is independent of the η-coordinate, and no singularity arises unless the radius of curvature R becomes infinite (the uniform slope case). It follows from (3.27) that, for $0 < \eta \ll c_1/K_1^2$, the time-averaged kinetic energy density above locally concave topography is given by

$$\frac{1}{4}\left|\frac{\partial\psi_T}{\partial\eta}\right|^2 \approx \frac{\epsilon^2K_1^4}{4c_1^2}. \tag{3.28}$$

This can be compared with the time-averaged kinetic energy density above locally convex topography (3.8) which, for $0 < \eta \ll c_1/4K_1^2$, is approximately equal to $\epsilon^2K_1^2/16c_1\eta$ [same as (3.10)]. Assuming that R and dh/dx (and therefore c_1) are the same at two given mooring sites, the first one being locally concave and the second one locally convex, we find that very close to the bottom, i.e., for $0 < \eta \ll c_1/4K_1^2 \approx (32s^2K_1^2R)^{-1}$,

$$\frac{(\text{K.E.})_{\text{concave}}}{(\text{K.E.})_{\text{convex}}} \approx \frac{(\epsilon^2K_1^4/4c_1^2)}{(\epsilon^2K_1^2/16c_1\eta)} = \frac{4K_1^2\eta}{c_1} \ll 1. \tag{3.29}$$

This suggests that close to the bottom, internal wave measurements made above locally concave topography are much less likely to show energy enhancement at the critical frequency than those made above locally convex topography. To understand why locally concave sites do not tend to show energy enhancement near ω_c, we first rewrite (3.24) as

$$\psi_T(\eta, t) = \psi_{Tr}(\eta, t) + \psi_{Tl}(\eta, t)$$

where

$$\psi_{Tr}(\eta, t) = -\epsilon \exp\left\{-i\left[K_1\left(\frac{\eta}{c_1}\right)^{1/2} + \omega t\right]\right\}, \quad 0 < \eta < \infty \tag{3.30}$$

$$\psi_{Tl}(\eta, t) = -\epsilon \exp\left\{i\left[K_1\left(\frac{\eta}{c_1}\right)^{1/2} - \omega t\right]\right\}, \quad 0 < \eta < \infty. \tag{3.31}$$

The above expressions for $\psi_{Tr}(\eta, t)$ and $\psi_{Tl}(\eta, t)$ are of the same form as (3.5) and (3.6), which were themselves shown to be consistent with Phillips' law of reflection for a bottom of uniform slope. This suggests we can interpret Baines' (1974) solution for the scattered wavefield (3.23)–(3.24) in terms of a series of specular reflections off the concave bottom. The first stage of these reflections occurs when the incident wave $\psi_i(\xi, t)$ impinges on $\xi = -(\eta/c_1)^{1/2}$ to generate $\psi_{Tr}(\eta, t)$, and on $\xi = (\eta/c_1)^{1/2}$ to generate $\psi_{Tl}(\eta, t)$. The second stage of reflections occurs when $\psi_{Tr}(\eta, t)$ impinges on $\xi = (\eta/c_1)^{1/2}$, and $\psi_{Tl}(\eta, t)$ impinges on $\xi = -(\eta/c_1)^{1/2}$ to generate $\psi_R(\xi, t)$. The situation is drawn schematically on Fig. 3.

Now if we let $K'(\eta)$ denote the local (WKB) value of the reflected wavenumber after the first reflection, we could proceed as we did for convex topography and show that the wavenumber amplification K'/K_1 is again given by (3.18). This result is not surprising in itself. What is interesting though is that for the second reflection, the wavenumber amplification K''/K' is equal to $-(K'/K_1)^{-1}$ for topography specified exactly by (3.20), due to the assumed symmetry of the reflecting surface with respect to ξ. This yields $K'' = -K_1$, and provides us with a simple explanation for the form of the back-reflected wave $\psi_R(\xi, t)$ given in (3.23).

The absence of a singularity in the velocity field near $\eta = 0$ is due to the fact that the wave reflected at $\xi = 0^+$ has a phase shift of π with respect to the wave reflected at $\xi = 0^-$, so that they interfere destructively. More generally, the wave ψ_{Tl} reflected at $\xi = (\eta/c_1)^{1/2}$ has a phase shift of $\pi + 2K_1(\eta/c_1)^{1/2}$ with respect to the wave ψ_{Tr} reflected at $\xi = -(\eta/c_1)^{1/2}$. We expect them to interfere constructively when

$$\pi + 2K_1\left(\frac{\eta}{c_1}\right)^{1/2} = 2n\pi, \quad n = 1, 2, 3, \cdots$$

$$K_1\left(\frac{\eta}{c_1}\right)^{1/2} = (2n-1)\frac{\pi}{2}, \quad n = 1, 2, 3, \cdots \tag{3.32}$$

When this condition is satisfied, we find that the velocity amplitude (3.26) for the total η-field of motion becomes twice that associated with ψ_{Tl} or ψ_{Tr} alone, as is indeed expected for constructive interference. This lends further support to our assertion that Baines' solution for the scattered wavefield (3.23)–(3.24) may be interpreted in terms of specular reflection theory.

We now summarize the key results of this section. For locally convex topography specified exactly by (3.2), the backscattered wave is identically zero. There is a singularity in energy density at $\eta = 0$, and the strength of this singularity is proportional to the local radius of curvature R of the topography. For η-characteristics which come directly in contact with the bottom (i.e., for $\eta < 0$), Baines' (1971b) solution for the scattered wavefield (3.5)–(3.6) is consistent in a WKB sense with the reflection law of Phillips (1977). For $\eta > 0$, there exists an evanescent field of oscillatory motions (3.4) whose origin cannot be explained by purely specular reflection, but there is no energy flux associated with it.

For locally concave topography specified exactly by (3.20), the back-reflected wave has the same amplitude as the incident wave, and the resulting field of motion is that of a standing wave. It is possible to interpret this solution in terms of a series of specular reflections off the concave bottom. Close to the origin (where $dh/dx \approx s$), ψ_{Tl} and ψ_{Tr} interfere destructively, and no singularity occurs. Locally concave topography is thus less likely to show energy enhancement near ω_c than locally convex topography.

4. Backscattered energy flux from a sharp convex corner

The topographic shapes considered in section 3 are highly idealized, being perfectly symmetric with respect to ξ, and with bottom slope at infinity asymptotic to that of the ξ-characteristics. Baines (1971b) briefly examined the effect of relaxing those two assumptions concerning the shape of the topography. He studied the problem of a wave incident on topography specified by (see Fig. 4)

$$\left.\begin{aligned} \eta &= -c_1\xi^2, && \xi_L < \xi < \xi_R \\ & && \xi_L < 0,\ |\xi_L| < \xi_R \\ \eta &= -c_1\xi_R(2\xi - \xi_R), && \xi > \xi_R \\ \eta &= -c_1\xi_L(2\xi - \xi_L), && \xi < \xi_L \end{aligned}\right\} \tag{4.1}$$

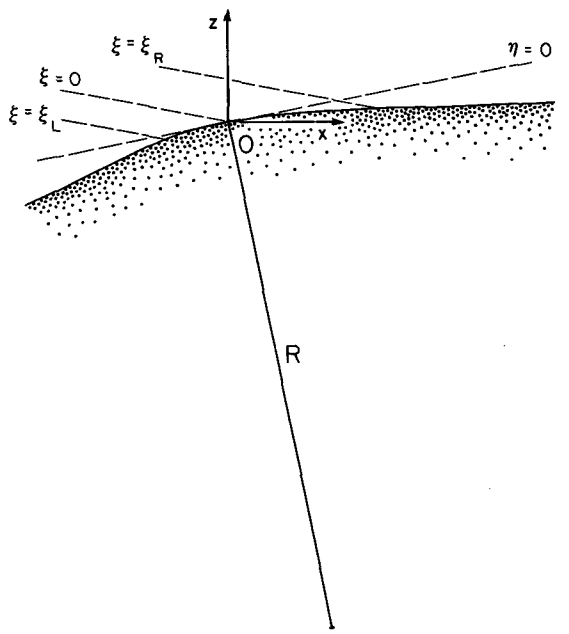

FIG. 4. Topographic shape described by (4.1). The bottom slope for $\xi > \xi_R (\xi < \xi_L)$ is given by (3.13) evaluated at $\xi = \xi_R (\xi = \xi_L)$.

where $c_1 = (1 + s^2)^{3/2}/8s^2R$ as before. Such topography is locally convex near the origin, but becomes plane on either side of it, with bottom slope a continuous function of ξ. Baines investigated the nature of the solution for the scattered wavefield near the origin and at large distances from it. He pointed out that the singularities [e.g., (3.9)] associated with the reflected waves are still present, so that we may still expect large energy and shear enhancement near ω_c for the topography shown on Fig. 4. He also found that the backscattered wave does not vanish near $\xi = 0$, and the velocity associated with it is finite and continuous there. However, while Baines pointed this out, he did not provide any estimate of the resulting backscattered energy flux.

Sandstrom (1972) also investigated the problem of a wave incident on a bottom where two asymptotically plane sections come together in a rounded corner. His method of solution uses specular reflection theory as a first approximation for the scattered wavefield, and then gets rid of the wave components which violate the radiation condition through a series of iterations. Among other things, he found that the amplitude of the backscattered wave is maximum for a sharp corner. Hence, we can obtain an upper bound for the backscattered energy flux from a rounded corner (e.g., Fig. 4) by letting R go to zero.

In this section, we use the theory developed by Hurley (1970) to evaluate the total energy flux which is backscattered from such a sharp corner. Because of the suggestion in (3.29) that convex corners are more likely to show energy enhancement near ω_c than concave corners, we are particularly interested in determining the backscattered energy flux for a sharp convex corner. A few changes to Hurley's algebra are needed to deal with the convex case. We only write the main results here in order to avoid introducing a great deal of new notation. The interested reader is referred to Hurley (1970) for a more detailed description of his theory.

We consider a fluid of constant buoyancy frequency N occupying the sector between two plane rigid walls OA and OB, where OA is horizontal and OB is inclined at an angle θ_B to it (Fig. 5). We want to determine the scattered wave field for an incident wave

$$\psi_i = \frac{U}{K} \exp[iK(x \sin\mu + z \cos\mu)] \qquad (4.2)$$

with velocity amplitude U and total wavenumber K, and where $\mu = \tan^{-1}s$ is the angle which the wave rays make with the horizontal. An $e^{-i\omega t}$ time dependence is understood but omitted in (4.2). The incident energy flux associated with ψ_i comes from the upper-left corner, rather than the upper-right corner as in Hurley (1970). The characteristic coordinates chosen by Hurley are

$$\sigma_+ = x \sin\mu - z \cos\mu$$

$$\sigma_- = x \sin\mu + z \cos\mu \qquad (4.3)$$

so that (4.2) could be more simply written as $\psi_i = U/K \exp(iK\sigma_-)$. Hurley's (σ_+, σ_-) coordinates are related to the (ξ, η) coordinates of Baines (1971b) as follows: $\sigma_+ = -\eta/(1 + s^2)^{1/2}$ and $\sigma_- = \xi/(1 + s^2)^{1/2}$. Thus, whereas $|\eta|$ and $|\xi|$ give us the vertical distance from the $\eta = 0$ and $\xi = 0$ characteristics respectively, $|\sigma_+|$

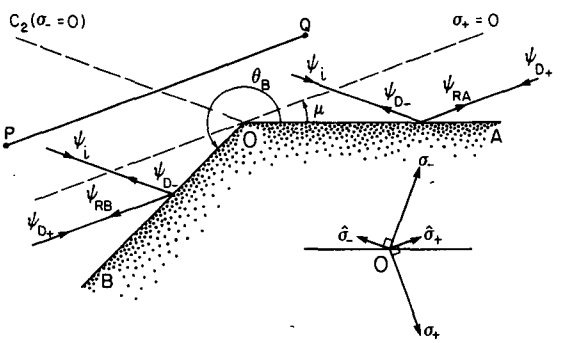

FIG. 5. A plane wave ψ_i is incident on convex, sharp-cornered topography. Pure specular reflection off OA(OB) would only give rise to the reflected wave $\psi_{RA}(\psi_{RB})$. However, diffracted waves (ψ_{D_+} and ψ_{D_-}) are also present due to the change in bottom slope at O. The direction of net energy flux for each of the waves is indicated by the arrows. The energy flux associated with ψ_{D_-} is evaluated along the path PQ, which lies on a σ_+ = constant line. The unit vectors $\hat{\sigma}_+$ and $\hat{\sigma}_-$ (4.12) are perpendicular to the σ_+ and σ_- axes (4.3) respectively.

and $|\sigma_-|$ give us the distance from these characteristics along a normal.

The wavefield generated by ψ_i is made up of the reflected waves ψ_{RA} and ψ_{RB} (Fig. 5), as well as the diffracted (or scattered) waves $\psi_{D_-}(\sigma_-)$ and $\psi_{D_+}(\sigma_+)$. Phillips' law of specular reflection yields the waves ψ_{RA} and ψ_{RB} for reflection off OA and OB. The diffracted waves ψ_{D_-} and ψ_{D_+} can be thought of as corrections to the Phillips solution. They cancel those wave components of ψ_{RA} and ψ_{RB} which carry energy toward the boundary and so violate the radiation condition (see Baines 1971a or Sandstrom 1972, for a more detailed discussion of this).

For the incident wave (4.2), it can be shown that equations (3.36) and (3.37) of Hurley (1970), derived now for a wave incident from the upper left, become

$$\psi'_{D_-}(\sigma_-) = -\frac{U\,\mathrm{sgn}(\sigma_-)}{c}\sinh\left[\frac{\pi^2}{c}\left(m_B+\begin{matrix}0\\1\end{matrix}\right)\right]\int_0^\infty \frac{\exp(-K|\sigma_-|t)dt}{\cos\left\{\frac{\pi}{c}\left[2\ln t + i\pi\left(2m - m_B + \begin{matrix}0\\1\end{matrix}\right)\right]\right\} - \cosh\left[\frac{\pi^2}{c}\left(m_B+\begin{matrix}0\\1\end{matrix}\right)\right]} \quad \text{for} \quad \sin(\theta_B+\mu) \gtrless 0 \tag{4.4}$$

$$\psi'_{D_+}(\sigma_+) = \frac{U\,\mathrm{sgn}(\sigma_+)}{c}\sinh\left[\frac{\pi^2}{c}\left(m_B+\begin{matrix}0\\1\end{matrix}\right)\right]\int_0^\infty \frac{\exp(-K|\sigma_+|t)dt}{\cos\left\{\frac{\pi}{c}\left[2\ln t + i\pi\left(-2n - m_B + \begin{matrix}1\\0\end{matrix}\right)\right]\right\} - \cosh\left[\frac{\pi^2}{c}\left(m_B+\begin{matrix}0\\1\end{matrix}\right)\right]}, \quad \text{for} \quad \sin(\theta_B+\mu) \gtrless 0 \tag{4.5}$$

where

$$c = \ln\left|\frac{\sin(\theta_B+\mu)}{\sin(\theta_B-\mu)}\right| - i(m_B+n_B)\pi, \tag{4.6}$$

m_B, n_B, and θ_B are the values which m, n, and θ take on the wall OB, according to the rules:

$$\left.\begin{aligned} m &= 0 \quad \text{for} \quad 0 < \theta < \pi - \mu \\ &= 1 \quad \text{for} \quad \pi - \mu < \theta < 2\pi - \mu \\ &= 2 \quad \text{for} \quad 2\pi - \mu < \theta < 2\pi \end{aligned}\right\} \tag{4.7}$$

and

$$\left.\begin{aligned} n &= 0 \quad \text{for} \quad 0 < \theta < \mu \\ &= 1 \quad \text{for} \quad \mu < \theta < \pi + \mu \\ &= 2 \quad \text{for} \quad \pi + \mu < \theta < 2\pi \end{aligned}\right\}. \tag{4.8}$$

Since we want to determine the backscattered energy flux for a convex corner, we are particularly interested in the case where θ_B lies in the range $\pi + \mu < \theta_B < 2\pi - \mu$. Equations (4.4)–(4.6) then become

$$\psi'_{D_-}(\sigma_-) = -\frac{U\,\mathrm{sgn}(\sigma_-)}{c}\sinh\left(\frac{2\pi^2}{c}\right)\int_0^\infty \frac{\exp(-K|\sigma_-|t)dt}{\cos\left\{\frac{\pi}{c}[2\ln t + i\pi(2m-1)]\right\} - \cosh\left(\frac{2\pi^2}{c}\right)} \tag{4.9}$$

and

$$\psi'_{D_+}(\sigma_+) = \frac{U\,\mathrm{sgn}(\sigma_+)}{c}\sinh\left(\frac{2\pi^2}{c}\right)\int_0^\infty \frac{\exp(-K|\sigma_+|t)dt}{\cos\left\{\frac{\pi}{c}[2\ln t - i\pi(2n+1)]\right\} - \cosh\left(\frac{2\pi^2}{c}\right)} \tag{4.10}$$

where

$$c = \ln\left|\frac{\sin(\theta_B+\mu)}{\sin(\theta_B-\mu)}\right| - 3i\pi.$$

The velocity associated with the diffracted wave is given by

$$\psi'_{D_-}\hat{\sigma}_- + \psi'_{D_+}\hat{\sigma}_+ \tag{4.11}$$

where $\hat{\sigma}_-$ and $\hat{\sigma}_+$ are unit vectors perpendicular to the σ_- and σ_+ axes respectively (Figure 5) and are given by

$$\hat{\sigma}_- = (-\cos\mu, \sin\mu)$$

$$\hat{\sigma}_+ = (\cos\mu, \sin\mu). \quad (4.12)$$

Now, let P and Q be two points at either end of a long line $\sigma_+ =$ constant (Fig. 5), and such that $\psi_i(\sigma_-)|_P = \psi_i(\sigma_-)|_Q$. We can then proceed as in Hurley (1970, Appendix) to show that the total, time-averaged backscattered energy flux in the direction of OC_2 is given by

$$\Delta\bar{P}_{C_2} = \frac{\rho_0\omega\cot\mu}{2}\int_{-\infty}^{+\infty} \mathrm{Im}\{\psi_{D-}\psi'^{*}_{D-}\}\,d\sigma_- \quad (4.13)$$

where ρ_0 is the undisturbed fluid density, Im{ } refers to the imaginary part of { }, and the asterisk denotes a complex conjugate. This expression can be evaluated numerically for any value of θ_B within its range of validity, i.e., $\pi + \mu < \theta_B < 2\pi - \mu$. The particular case where $\theta_B = \pi + 2\mu$ is interesting, because the wave rays associated with ψ_{RA} and ψ_{RB} then make the same angle μ with respect to OA and OB respectively. For this "symmetric case," the backscattered energy flux is nearly constant for $\mu \leq 10°$, and is given by

$$\Delta\bar{P}_{C_2} = (0.048)\,U^2K^{-2}\rho_0\omega\cot\mu. \quad (4.14)$$

The backscattered energy flux slowly decreases for larger values of μ, but is only 10% smaller for $\mu = \pi/4$, $\theta_B = 3\pi/2$. Numerical integrations performed for the nonsymmetric case ($\theta_B \neq \pi + 2\mu$) yield similar estimates of the backscattered energy flux. We can compare $\Delta\bar{P}_{C_2}$ to the time-averaged energy flux $\bar{P}_i$ which is incident over one wavelength:

$$\bar{P}_i = \frac{\rho_0\omega\cot\mu}{2}\int_{-\pi/K}^{\pi/K} \mathrm{Im}\{\psi_i\psi'^{*}_i\}\,d\sigma_- \quad (4.15)$$

$$= -\frac{U^2\rho_0\omega\cot\mu}{2K}\int_{-\pi/K}^{\pi/K} d\sigma_-$$

$$\bar{P}_i = -\pi\,U^2K^{-2}\rho_0\omega\cot\mu. \quad (4.16)$$

Dividing (4.14) by (4.16), we find that the total backscattered energy flux (integrated from $\sigma_- = -\infty$ to $\sigma_- = +\infty$) is equivalent to only 1.5% of the energy flux incident in a beam of width equal to one wavelength. On that basis alone, we may be justified to say that $\Delta\bar{P}_{C_2}$ is small enough to be neglected, especially as it represents an upper bound for the energy flux that might be backscattered from a rounded convex corner.

However, we note that the dissipated energy flux F_d (Fig. 1), as evaluated by GG, also represents only a small percentage of the typical downward incident energy flux of about 20–30 mW m^{-2} in the ocean (Eriksen 1985). Consequently, if the total backscattered energy flux for a rounded convex corner were as large as for a sharp convex corner, and if it occurred mostly in the region where $dh/dx \approx s$, large wavenumber amplifications (3.18) may no longer be possible, and this would affect GG's estimates of F_d. To illustrate this point for the specific case of the rounded convex corner drawn on Fig. 4, we shall assume that the total backscattered energy flux has the same magnitude as (4.14), and further assume that it all occurs within $\pm 0.015/2$ wavelength of the $\xi = 0$ characteristic. For this hypothetical, worst case scenario, the incident waves are completely backscattered in a beam of width 0.015 wavelength centered about $\xi = 0$, and are specularly reflected outside that region. The largest wavenumber amplification then possible (3.16) would be

$$\left|\frac{K'}{K}\right| \approx \frac{85s^2(KR)}{(1+s^2)^{3/2}}. \quad (4.17)$$

Now in the model of GG, where j denotes an incident vertical modenumber, and j_p denotes the cutoff modenumber such that $\mathrm{Ri}^{-1}(j_p) = 1$, the only waves assumed to break and dissipate are those for which $|K'/K| > j_p/j$. According to that model then, energy dissipation requires

$$KR > \left(\frac{j_p}{j}\right)\frac{(1+s^2)^{3/2}}{85s^2}. \quad (4.18)$$

For typical values of j_p ranging from 30 to 100 (GG, Fig. 5), low modes j, and small values of the wave ray slope ($0.01 < s < 0.10$, say), (4.18) then suggests that we need $KR \gg 1$ in order to avoid significant reductions of the dissipated energy flux F_d. For the lowest vertical modes of the incident wavefield (Munk, 1981) which carry most of the incident energy flux, $K = O(10^{-3}$ m$^{-1})$, and this requires a radius of curvature R of the order of several tens of kilometers or more. Thus according to the worst case scenario presented above, very large values of R would seem to be necessary if we wish to totally ignore scattering effects in evaluations of F_d.

A more generous criterion than (4.18) can probably be obtained, provided (i) the total backscattered energy flux for a rounded convex corner is less than (4.14) derived for a sharp convex corner, and (ii) does not occur exclusively near $\xi = 0$ (where $dh/dx \approx s$), but is more evenly distributed over the entire region of nonuniform slope (e.g., $\xi_L < \xi < \xi_R$ for Fig. 4).

The work of Sandstrom (1972) lends some credence to (i). It does not allow us to make any statement about (ii) however, because the topography profile considered in his paper has $dh/dx < s$ everywhere, and is locally concave. Yet it can be argued that for a rounded corner, since the change in bottom slope oc-

curs over a broad area rather than at a single location, the backscattered energy flux should be more uniformly distributed in space than for a sharp corner, so that (ii) seems plausible too.

As a rough criterion, the results of Sandstrom (1972) suggest that internal wave scattering off an isolated, rounded corner, can be adequately described by specular reflection theory when R is comparable to or larger than the incident wavelength ($KR \geq 1$). We do not know whether this criterion would remain valid for more realistic topographic shapes, where several "corners" with different radii of curvature may be present at once for instance. If it did, the implications for ocean mixing would be important. For the typical oceanic internal wavefield (Munk 1981), we would expect all incident waves to be specularly reflected when R is only of the order of a few kilometers or more. An interesting question then is to ask how the reflected wavefield might vary with height above the bottom over a convex portion of the topography.

5. Kinematic effects of finite topography

Referring to Fig. 6, we suppose the anchor weight of a mooring line is at A, where the bottom slope is $\tan\alpha$ and the local radius of curvature is equal to R.

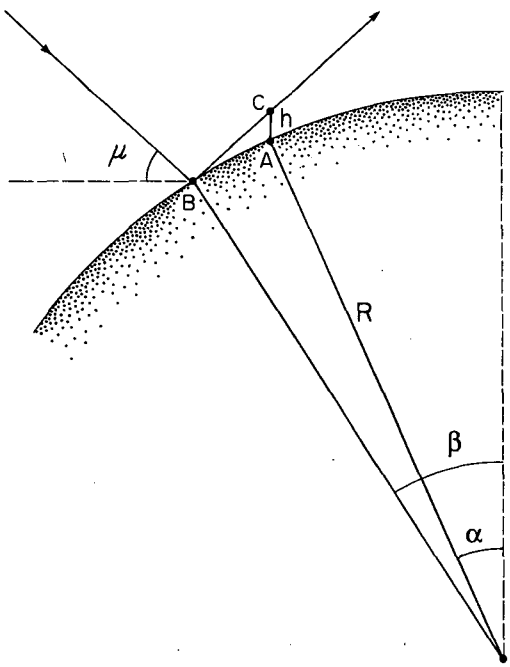

FIG. 6. A mooring line is deployed over locally convex topography. Its anchor weight lies at A, where the bottom slope is $\tan\alpha$ and the radius of curvature is equal to R. A wave ray inclined at an angle μ with respect to the horizontal impinges on the bottom at B, where the local slope is $\tan\beta$. The reflected wave ray intersects our mooring line at C, some height h above the bottom.

For the sake of simplicity, we assume R = const, and allow a single azimuthal angle of incidence ($\phi_i = 0$ for onshore propagation of energy, following Eriksen 1982). All internal wave frequencies ($f < \omega < N$) are allowed to be incident on the bottom however.

Suppose our mooring line has a sensor (e.g., current meter) at C, some height h above the bottom. Not all reflected rays will intersect our sensor, but one that does is drawn on Fig. 6. It is inclined at an angle μ with respect to the horizontal determined by its frequency, and impinges on the bottom at B where the bottom slope is $\tan\beta$. Simple geometry shows that the angle β is given by

$$\beta = \cos^{-1}\left\{\cos(\alpha - \mu) + \frac{h}{R}\cos\mu\right\} + \mu. \quad (5.1)$$

For any specific instrument on a mooring line, the parameters $\tan\alpha$ and h/R are constant, so that (5.1) essentially gives us β as a function of μ. Critical reflection occurs when $\beta = \mu = \mu_c$, in which case (5.1) reduces to

$$\cos(\alpha - \mu_c) + \frac{h}{R}\cos\mu_c = 1. \quad (5.2)$$

Right on the bottom ($h = 0$), this yields $\mu_c = \alpha$, as expected. However, at some height h above the bottom, μ_c can take two values. The smaller one ($\mu_c < \alpha$) results from critical reflection at a point shallower than A, whereas the larger one ($\mu_c > \alpha$) results from critical reflection at a point deeper than A. Both values of μ_c satisfy (5.2) and can be found by iteration for given values of $\tan\alpha$ and h/R. The frequencies corresponding to these values of μ are easily obtained from the dispersion relation, which we write as

$$\frac{\omega}{f} = \left[\frac{1 + (N/f)^2\tan^2\mu}{1 + \tan^2\mu}\right]^{1/2}. \quad (5.3)$$

The linear inviscid theory of Phillips (1977) predicts an infinite wavenumber amplification (3.19) for critical reflection ($\mu = \beta$), and therefore an infinite energy density amplification E'/E. Figure 7 shows how the frequency of critically reflected waves varies with height above the bottom, for the particular case where $N/f = 13.1$ and $\tan\alpha = 0.30$, as proposed by Eriksen (1982) for Muir Seamount mooring 518. Using (5.1), we can also find two values of μ (and hence ω) for which the wavenumber amplification (3.19) equals $\sqrt{10}$, so that the reflected energy density E' is 10 times greater than the incident energy density E. The frequency for which $E'/E = 10$ varies with height above the bottom, and this is also shown on Fig. 7.

Figure 8 presents the same information as Fig. 7, but for $\tan\alpha = 0.125$ instead of 0.30 [the bottom slope at mooring 518 probably lies somewhere between 0.10

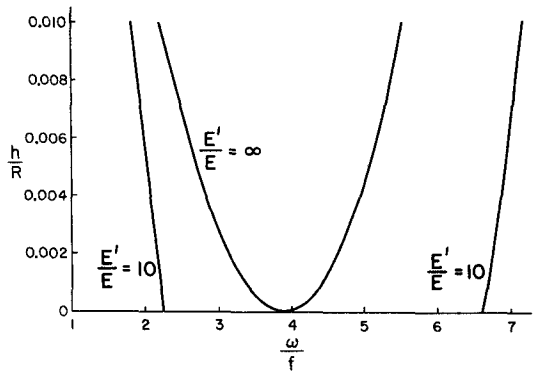

FIG. 7. Variation of the reflected energy spectrum with height above the bottom for the idealized topography shown on Fig. 6, taking $\tan\alpha = 0.30$ and $N/f = 13.1$, as proposed by Eriksen (1982) for Muir Seamount mooring 518. The energy density amplification E'/E is given by the square of the wavenumber amplification (3.19).

and 0.20 (Wunsch 1976, Fig. 5)]. On linear inviscid grounds alone, both figures predict a rapid evolution of the reflected energy spectrum with height above the bottom, with some sensitivity on the choice of $\tan\alpha$. For $\tan\alpha = 0.125$ for example, the critical frequency at $h = 0$ is $\omega_c = 1.9f$, close to the M_2 tidal frequency. Merely 100 m above the bottom, taking $R \approx 30$ km yields $h/R \approx 0.003$, and Fig. 8 then predicts enhanced energy densities over a broad range of frequencies for $\omega \geq 2.8f$, and over a very narrow range of frequencies for $\omega \approx 1.2f$.

It could be argued that the singularities associated with critically reflected waves at $\omega = 1.2f$ and $\omega = 2.8f$ are wiped out immediately upon reflection due to shear instability, following the scenario proposed by GG. The elimination of those shear unstable waves would leave a residual energy spectrum very different from the canonical Garrett–Munk spectrum, in both wavenumber and frequency space (e.g., GG, Fig. 8). Nonlinear interactions among internal waves could then start reshaping this perturbed spectrum before its energy signature has time to reach our sensor. The extent of the spectral readjustment would presumably depend in some complicated way on the oblique distance (e.g., $\overline{BC}$ on Fig. 6) between our sensor and the underlying bottom, itself a function of frequency.

The observed spectrum (Eriksen 1982, Fig. 3) has enhanced energy densities over a broad range of frequencies starting at about $\omega = 2.8f$, but centered at $\omega \approx 4f$. It also has enhanced energy density over a very narrow range of frequencies near $\omega \approx 1.7f$, perhaps due to local generation of the M_2 internal tide. Those observations do not agree in detail with the prediction of Fig. 8 for $h/R \approx 0.003$, but the gross pattern of spectral enhancement agrees reasonably well though, given the simplifications made about the shape of the topography.

Our main objective in presenting the above model was simply to point out that current meters (or other sensors) placed at different heights above a nonuniformly sloping bottom do not feel the same topography. Therefore, in addition to nonlinear and viscous effects, finite topographic effects could play a role in the rapid change with height of internal wave spectra observed by Eriksen (1982) at a few mooring sites. To carefully determine the importance of finite topographic effects at a particular site (e.g., mooring 518 above), we would have to relax our assumption that R = const. We may also have to consider the truly three-dimensional nature of the topography and the incident wavefield, which we ignored in this paper. Since the Garrett–Munk internal wave spectrum is isotropic, that would imply allowing for waves to be incident at any angle with respect to the isobaths (i.e., $\phi_i = -\pi, \pi$ instead of just $\phi_i = 0$). It would also imply allowing for alongslope variations of the topography.

6. Discussion and conclusions

Internal wave measurements made in the first 100 m or so above sloping bottoms often depart noticeably from the canonical Garrett–Munk model spectrum (Wunsch 1976; Wunsch and Webb 1979). However, the extent of this departure is highly variable, presumably because of the often complicated shape of the underlying sea floor. This is especially true in the neighborhood of the critical frequency ω_c; there are locations where energy enhancement near ω_c is very noticeable (Eriksen 1982), and others where it is absent (Thorpe 1987). We believe some of this variability can be explained in terms of the solutions found by Baines (1971b, 1974) for the idealized bottom shapes of section 3. Those solutions lead to (3.29), which suggests that internal wave measurements made above locally concave topography are less likely to show energy en-

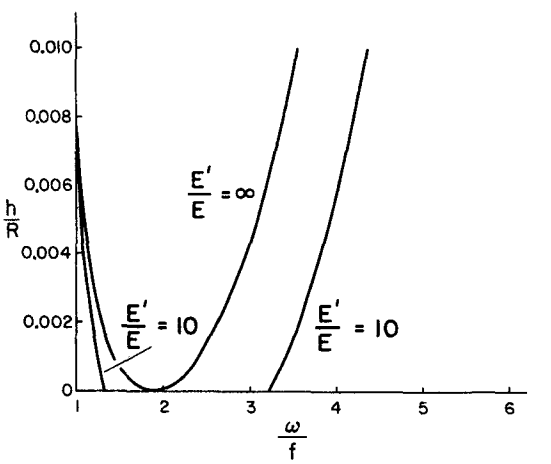

FIG. 8. As in Fig. 7, but for $\tan\alpha = 0.125$.

hancement near ω_c than similar measurements made above convex topography.

There is at least some observational support for this claim. Thorpe (1987) made detailed near-bottom measurements of temperature, salinity, and currents in a locally concave portion of the continental slope southwest of Ireland, and found no statistically significant enhancement of energy density near ω_c. Similarly, the measurements of Wunsch and Hendry (1972) showed no obvious energy enhancement near ω_c over the concave portion of the continental slope (e.g., at moorings 352 and 351) south of Cape Cod. On the other hand, measurements made above a convex portion of the very same continental slope (e.g., at mooring 348 where the distance between isobaths increases shoreward) exhibit enhanced energy density near ω_c (Eriksen 1982, Fig. 4).

The most convincing evidence of energy and shear amplification near ω_c (Eriksen 1982) comes from a site which does not appear to be either concave or convex, however. Mooring 636 of the Western Boundary Sill Experiment (WBSE) was deployed at 4°2.5′N, 39°40.5′W, near the midpoint of a 10 km long stretch of sea floor with "constant" slope $dh/dx \approx 0.015$ (Whitehead and Worthington 1982, Fig. 4). The radius of curvature R of the topography is probably of the order of several tens of kilometers there, although a reliable estimate of it cannot be obtained from available bathymetric data. With $KR \gg 1$ for the whole incident internal wave spectrum, all incident waves should be reflected as if from an infinite sloping plane. Consequently, GG's estimate of the dissipated energy flux (F_d) should be unaffected by diffraction at mooring 636.

This example illustrates the fact that even abyssal hills of modest height ($\approx$300 m in the above case) can exhibit significant energy and shear enhancement near the critical frequency, provided they have large radii of curvature. Figure 9 of GG thus overemphasized the reductions in F_d that might result from internal wave reflection off the side of small-scale features on the ocean floor. The immediate implication of this for ocean mixing is that it may be possible to obtain a reasonably high basin-averaged value of F_d due to the steepness of abyssal hills, with much of the sensitivity coming from the f/N dependence of F_d (Fig. 1). A rough measure of the steepness of random abyssal hills can be obtained from the empirical topographic spectrum of Bell (1975b, p. 884), which suggests an rms bottom slope of 0.03, 0.07, and 0.16 when integrated up to wavenumbers 0.1 cycle km^{-1}, 0.5 cycle km^{-1}, and 2.5 cycle km^{-1} respectively.

We now summarize the main conclusions of our paper:

1) Close to the bottom, locally convex sites are more likely to show energy enhancement near ω_c than concave sites, suggesting that energy dissipation rates associated with the breaking of internal waves should also be higher above locally convex topography.

2) The total energy flux backscattered from a sharp convex corner amounts to 1.5% of the energy flux incident over a single wavelength. A worst case scenario based on this result suggests that energy backscattering can be safely ignored in estimates of F_d only when $KR \gg 1$. However, we point out that if the results of Sandstrom (1972) can be extended to the case of a rounded convex corner, we might be allowed to neglect scattering effects for $KR \gtrsim 1$, a clearly more generous criterion.

3) For nonuniformly sloping topography, rapid variations of the reflected energy spectrum with height above the bottom can be explained in terms of linear, inviscid, specular reflection theory. Therefore, in addition to nonlinear and viscous effects, the finite scale of topography could play a role in the rapid change with height of internal wave spectra observed by Eriksen (1982) at a few mooring sites.

As a rough working hypothesis, we suggest that topography be smoothed over a scale of a few km, and that the dissipated energy flux F_d then be taken as zero in concave regions, and given by the GG formula (see Fig. 1 here) in convex regions. Further energy dissipation may, of course, occur due to the non-linear relaxation of the GG residual spectrum.

Acknowledgments. We thank Hal Sandstrom for discussion and several useful suggestions during the course of this work. The patience of Jackie Hurst in TEXing this manuscript was also greatly appreciated. We are partially supported by the U.S. Office of Naval Research under Contract N00014-87-G-0028 and by Canada's Natural Sciences and Engineering Research Council.

REFERENCES

Baines, P. G., 1971a: The reflexion of internal/inertial waves from bumpy surfaces. *J. Fluid Mech.*, **46**, 273–291.

——, 1971b: The reflexion of internal/inertial waves from bumpy surfaces. Part 2: Split reflexion and diffraction. *J. Fluid Mech.*, **49**, 113–131.

——, 1974: The generation of internal tides over steep continental slopes. *Phil. Trans. Roy. Soc. London*, Ser. A, **277**, 27–58.

Bell, T. H., 1975a: Topographically generated internal waves in the deep ocean. *J. Geophys. Res.*, **80**, 320–327.

——, 1975b: Statistical features of sea-floor topography. *Deep-Sea Res.*, **22**, 883–892.

Eriksen, C. C., 1982: Observations of internal wave reflection off sloping bottoms. *J. Geophys. Res.*, **87**, 525–538.

——, 1985: Implications of ocean bottom reflection for internal wave spectra and mixing. *J. Phys. Oceanogr.*, **15**, 1145–1156.

Garrett, C. J. R., and D. Gilbert, 1988: Estimates of vertical mixing by internal waves reflected off a sloping bottom. *Small-Scale Turbulence and Mixing in the Ocean.* J. C. J. Nihoul and B. M. Jamart, Eds., Elsevier, pp. 405–423.

Gill, A. E., 1982: *Atmosphere-Ocean Dynamics.* Academic Press, 662 pp.

Hurley, D. G., 1970: Internal waves in a wedge-shaped region. *J. Fluid Mech.*, **43,** 97–120.

Longuet-Higgins, M. S., 1969: On the reflection of wave characteristics from rough surfaces. *J. Fluid Mech.*, **37,** 231–250.

Mied, R. P., and J. P. Dugan, 1976: Internal wave reflexion from a sinusoidally corrugated surface. *J. Fluid Mech.*, **76,** 259–272.

Munk, W. H., 1981: Internal waves and small-scale processes, *Evolution of Physical Oceanography Scientific Surveys in Honor of Henry Stommel.* B. A. Warren and C. Wunsch, Eds., M.I.T. Press, pp. 264–291.

Olbers, D. J., 1983: Models of the oceanic internal wavefield. *Rev. Geophys. Space Phys.*, **21,** 1567–1606.

Phillips, O. M., 1977: *The Dynamics of the Upper Ocean.* 2nd ed., Cambridge University Press, 336 pp.

Rubenstein, D., 1988: Scattering of inertial waves by rough bathymetry. *J. Phys. Oceanogr.*, **18,** 5–18.

Sandstrom, H., 1966: The importance of topography in generation and propagation of internal waves. Ph.D. thesis, University of California at San Diego.

——, 1972: The effect of boundary curvature on reflection of internal waves. *Mém. Soc. R. Sci. Liège,* 6ème sér., tome IV. *Fourth Liège Colloq. on Ocean Hydrodynamics.* J. C. J. Nihoul, Ed., pp. 183–190.

Thorpe, S. A., 1987: Current and temperature variability on the continental slope. *Phil. Trans. Roy. Soc. London,* Ser. A, **323,** 471–517.

Whitehead, J. A., and L. V. Worthington, 1982: The flux and mixing rates of Antarctic Bottom Water within the North Atlantic. *J. Geophys. Res.*, **87,** 7903–7924.

Wunsch, C., 1976: Geographical variability of the internal wavefield: A search for sources and sinks. *J. Phys. Oceanogr.*, **6,** 471–485.

——, and R. Hendry, 1972: Array measurements of the bottom boundary layer and the internal wave field on the continental slope. *Geophys. Fluid Dyn.*, **4,** 101–145.

——, and S. Webb, 1979: The climatology of deep ocean internal waves. *J. Phys. Oceanogr.*, **9,** 235–243.